Structural and Electrochemical Characterization of Immobilized Polymerized Electroactive Vesicles

I. Stanish,* D. A. Lowy,† Y. Lee, J. Fang, E. Wong, R. I. Ray, and A. Singh

Center for Bio/Molecular Science and Engineering, Naval Research Laboratory, Code 6930, Washington, D.C. 20375

Received: July 29, 2003; In Final Form: October 15, 2003

Immobilized polymerized electroactive vesicles (IPEVs) are biocapsules capable of storing charge in confined environments and of chemisorbing on conductive metal surfaces. Methods to immobilize stable electroactive vesicles and the means to measure their electroactivity at nanocoulomb levels are demonstrated. Charge transport between the electrode surface and the vesicle interior is tuned by adjusting the concentration of a membrane-soluble electron mediator. IPEVs serve as a model for developing biomimetic systems intended for charge storage and electron coupling applications.

1. Introduction

Polymerized vesicles[1] have been demonstrated primarily in the bulk phase as a biomimetic system capable of carrying out cell-like functions.[2] Such advances relevant to electrochemical processes include charge storage,[3] electron transport,[4] electron hopping,[5] and electron conduction.[6] For electron coupling applications,[7] immobilizing electroactive vesicles onto conducting surfaces to exploit these aforementioned electrochemical events would be advantageous. Several investigators have immobilized vesicles on surfaces using such techniques as oligonucleotide assembly,[8] layer-by-layer polyelectrolyte assembly,[9] avidin−biotin binding,[10] hydrophobic binding,[11] and attractive surface-polarizable binding.[12] However, these systems do not demonstrate mediated electron transport between immobilized vesicles and its solid support. Our previous work based on sulfur−gold chemisorption of polymerized vesicles[13] is one example which can serve as an architectural model for electron exchange between the vesicle interior and the electrode surface. In this paper, we present a means by which to tailor vesicles for interfacial charge storage and charge transport. Our design is schematically depicted in Figure 1A, with component chemical structures provided in Figure 1B. Unilamellar vesicles that encapsulate potassium ferricyanide within their aqueous core and incorporate 1,4-benzoquinone (BQ) within their lipid bilayer membrane are partially polymerized and chemisorbed to a gold surface. The strong sulfur−gold dative bond drives the surface assembly of electroactive vesicles, while a short alkyl tether provides a proximal link for facile electron exchange between immobilized vesicles and the gold surface via the membrane-bound electron mediator. In this article, immobilized polymerized electroactive vesicles (IPEVs) are evaluated from both a materials science and an electrochemical perspective for their charge storage and charge transport properties.

2. Experimental Protocol

2.1. Materials. Unless stated otherwise, all reagents and chemicals were obtained commercially and used without further purification. Organic and dueterated solvents, potassium hydroxide, potassium salts, iodine, silica (200−400 mesh), and 1,4-benzoquinone were purchased from Aldrich (Milwaukee, WI). High purity monensin sodium salt was obtained from Calbiochem (San Diego, CA). Phosphomolybdic, Dragendorf's reagent, molybdenum stain, and monobasic sodium phosphate were purchased from Sigma (St. Louis, MO). 1,2-Bis(10,12-tricosadiynoyl)-*sn*-glycero-3-phosphatidylethanolamine ($DC_{8,9}PE$) was purchased from Avanti (Alabaster, AL). 2-Bis(10,12-tricosadiynoyl)-*sn*-glycero-3-phosphatidylcholine ($DC_{8,9}PC$) was synthesized according to previously published procedures.[14] *N*-Succinimidyl 3-[2-pyridyldithio]proprionate (SPDP) was purchased from Pierce (Rockford, IL). All solutions were prepared with deionized water (18 Mohm cm) using a Millipore-Q system.

2.2. Lipid Synthesis and Characterization. *N*-3-(Pyridyl-2-dithio)propionyl-2-bis(10,12-tricosadiynoyl)-*sn*-glycero-3-phosphatidyethanolamine (PDP-$DC_{8,9}PE$) was synthesized via a modified version of an established protocol for phosphatidylethanolamine/succinimidyl coupling.[15] An 80 mg (91.7 μmol) sample of vacuum-dried $DC_{8,9}PE$ dissolved in 9 mL of anhydrous pyridine and 35 mg (112 μmol) of SPDP dissolved in 5 mL of anhydrous pyridine was stirred under N_2 at room temperature in a water dish overnight and covered with aluminum foil. After evaporation of the solvent, the residue was redissolved in 500 μL of $CHCl_3$ and purified by gradient chromatography using 20 g of silica with the following mobile phase compositions: 100:0, 90:10, 80:20, 70:30 $CHCl_3$:MeOH. The product fractions were collected and then filtered to remove residual silica particles. The solvent was evaporated to provide 63% yield of product having an R_f of 0.74 eluting with 70:30 $CHCl_3$:MeOH. PDP-$DC_{8,9}PE$ was characterized by ^1H nuclear magnetic resonance spectroscopy (Bruker, 400 MHz) referenced with respect to internal TMS in $CDCl_3$ and by electrospray mass spectrometry in negative ion mode using a Finnigan Thermoques LCQ quadrupole ion trap. ^1H NMR ($CDCl_3$): δ 8.45 (s(b), *o*-pyridine), 7.67 (m, 2H *m*-pyridine), 7.12 (m, 1H *p*-pyridine), 5.21 (s(b), 1H >C*H*−), 4.36, 4.13 (m, 2H >CH−CH_2−OOC), 3.92 (m, 4H −CH_2−OPO−CH_2−), 3.47 (m, 2H −S−CH$_2$−CH_2−CONH−), 3.1 (m, 2H −CONH−CH_2−CH$_2$−OPO−), 2.71 (m, 2H −S−CH_2−CH$_2$−CONH−),

* Corresponding author. Telephone: (202) 404-6123. Fax: (202) 767-9594. E-mail: istanish@cbmse.nrl.navy.mil.

† Nova Research, Inc., 1900 Elkin St., Alexandria, VA 22308.

10.1021/jp0362234 CCC: $27.50
Published on Web 12/05/2003

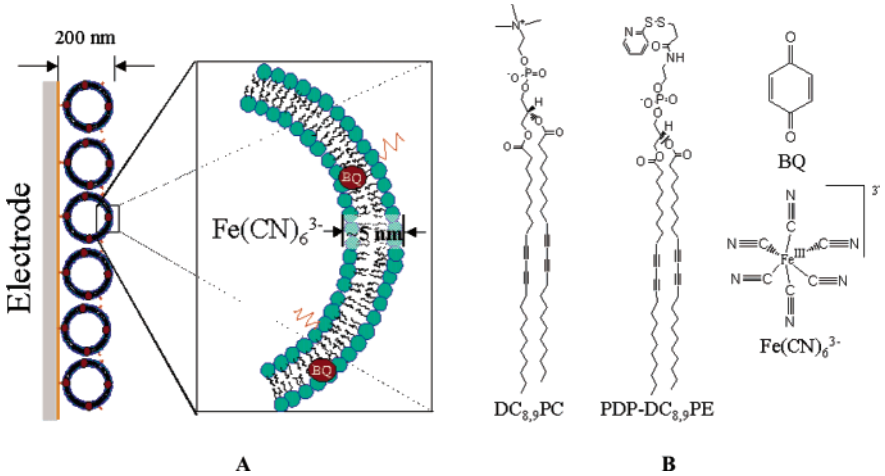

Figure 1. Schematic (not drawn to scale) of an IPEV electrode. (A) A mercaptoethyl tether anchors polymerized electroactive vesicles on a conducting gold surface. Electrons flow reversibly from the electrode to the entrapped electron acceptor ($Fe(CN)_6^{3-}$) shuttled by an electron mediator (1,4-benzoquinone) which also transports protons to maintain electrical neutrality. (B) Chemical structures of polymerizable $DC_{8,9}PC$ (major component) and PDP-$DC_{8,9}PE$ (minor component) lipids and electroactive components incorporated within the vesicle core ($Fe(CN)_6^{3-}$) and membrane (1,4-benzoquinone).

2.24 (t, 12H $-OOC-CH_2-$; $-CH_2-CCCC-CH_2-$), 1.52 (t, 12H $-OOC-CH_2CH_2-$; $-CH_2-CH_2-CCCC-CH_2-CH_2-$), 1.29 (m, 46H $-CH_2-$), 0.89 (t, 6H $-CH_3$). m/z = 1068. Differential scanning calorimetry (DSC-7 Perkin-Elmer) was used to determine the chain melting temperature for the monomeric lipid. A 3.34 mg sample of PDP-$DC_{8,9}PE$ was hydrated with 30 μL of H_2O at 50 °C and then scanned twice from 5 to 95 to 5 °C at a rate of 5 °C/min, giving a T_m of 27.2 °C (Endotherm, ΔH = 55.2 J/g). At 3 mol %, PDP-$DC_{8,9}PE$ mixed cooperatively with $DC_{8,9}PC$; the T_m of the mixture is 42 °C, near that of pure $DC_{8,9}PC$.[16]

2.3. Vesicle Synthesis and Characterization. A 10 mL volume of $CHCl_3$ was added to a round-bottom flask containing dried $DC_{8,9}PC$ lipids (25 mg, 27.3 μmol) and 100 μL of 9.36 mM PDP-$DC_{8,9}PE$ dissolved in $CHCl_3$ (1.04 mg, 0.936 μmol), evaporated under reduced pressure, and subsequently dried under high vacuum for 2 h. A dispersion (5 mL) of vesicles in 1 mM $K_3Fe(CN)_6$ consisting of $DC_{8,9}PC$ at 5 mg/mL doped at 3 mol % with PDP-$DC_{8,9}PE$ was incubated at 50 °C and sporadically vortexed for 3 h (in the dark, under N_2) and then extruded 10 times at 50 °C through a 0.6 μm and then through a 0.2 μm Nucleopore membrane using a Lipex extruder (Lipex Biomembranes Inc., Vancouver BC). Extravesicular ferricyanide was removed by anion exchange chromatography (Amberlite, 1.1 × 12 cm column height) using 2 mM KCl as the mobile phase. Eluted vesicles were rapidly cooled to 3.8 °C for 10 s and then immediately photopolymerized by irradiation at 254 nm for 3 min in a Rayonet Photochemical reactor equipped with sixteen 35 W Hg lamps (South New England Ultraviolet Co., Hamden, CT). Stained vesicles were examined using a Hitachi 8100 high-resolution transmission electron microscope (HR-TEM) and a Zeiss EM-10 transmission electron microscope to determine vesicle size (submicron), shape (spherical), and lamellarity (uni-). One drop of vesicle dispersion was added to the copper side of the carbon−copper grid, and then one drop of 1% w/w uranyl acetate was added for 3 min and then wicked away using a chem-wipe.

2.4. Surface Synthesis and Characterization. Gold films were deposited using an Edwards Auto306 thermal evaporator (Edwards High Vacuum, West Sussex, UK). Glass slides previously cleaned with an alkaline detergent (RBS-35, Pierce, Rockford, IL) were rinsed with ethanol, dried with N_2, and then mounted in the vacuum chamber. Pressure was established at 10^{-6} Torr prior to metal deposition. A precursor film of chromium metal (7 nm) was deposited onto the glass. Gold was deposited onto the precursor film to a thickness of 70 nm with a typical surface roughness of 2.2 nm.[13a] Gold disk electrodes (0.04 cm^2 effective area, Bioanalytical Systems, BAS, Lafayette, ID) were polished with alumina and diamond paste, sonicated in ethanol for 15 min, and then electrochemically activated in 0.1 M H_2SO_4 by applying 0.2 s potential pulses for 30 cycles at ±3 V vs Ag|AgCl, sat. KCl. Quartz crystal microbalance resonator crystals were rinsed with 5% HCl in ethanol and then with deionized water followed by drying with N_2.

2.5. Material Characterization of IPEVs. A Model USI-100 quartz crystal microbalance (QCM, Sanwa Tsusho Co., Tokyo, Japan) linked with a Hewlett-Packard 53131A, 225 MHz universal counter, was used. Measurements were carried out using 0.340 in. diameter gold-plated crystals having a fundamental frequency of 9 MHz. The procedure for vesicle deposition was the following: a 30 μL aliquot of vesicle dispersion was placed on a clean QCM resonator for 5 min, rinsed with water, and then dried with a stream of N_2. This sequence was repeated several times. Atomic force microscopy (AFM, Nanoscope IIIa, Digital Instruments) was used to image the vesicle structures immobilized on gold crystal resonators. All measurements were performed in air at room temperature using tapping mode. The line scan speed was 2 Hz with 512 pixels. To minimize drift during imaging, the microscope and sample were allowed to thermally stabilize for 20 min. Environmental scanning electron microscopy (ESEM) was carried out in an Electroscan Model E3 microscope (Wilmington, MA). Sample substrates (also from the same gold crystal resonator) were attached to a refrigerated Peltier stage maintained at 4 °C and imaged in an environment of water vapor (2−5 Torr). ESEM was operated at 20 keV using the environmental secondary electron detector. Energy dispersive spectroscopy (EDS) data were obtained with a NORAN Series II system microanalyzer (Middleton, WI) equipped with a beryllium window. Samples were held at a 20° tilt during spectra acquisition. X-ray fluorescence spectroscopy (XRFS) was conducted on thermally evaporated gold film substrates using an EDX-771 (Thermo-Electron, Scotts Valley, CA).

2.6. Electrochemical Characterization of IPEVs. Polymerized vesicles that encapsulate 1 mM ferricyanide or distilled water for control experiments were immobilized (deposition time

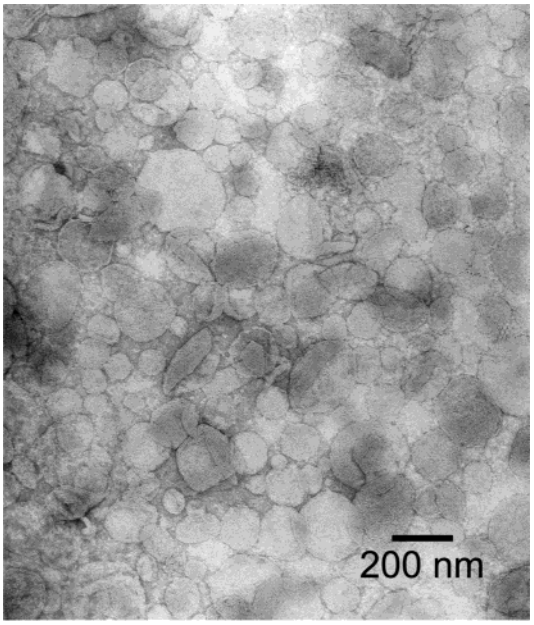

Figure 2. TEM image of polymerized vesicles that encapsulate 1 mM $K_3Fe(CN)_6$ prior to immobilization.

30 min) on clean gold disk working electrodes (WE). Electroanalytical measurements were performed using a Model 660 electrochemical workstation (CH Instruments, Austin, TX) equipped with Faraday cage. WE was used in conjunction with a Pt-coated Nb wire counter electrode (CE) and a miniaturized reference electrode (MRE).[17] Unless stated otherwise, all potentials are referenced with respect to MRE. The formal potential of MRE is -0.036 ± 0.002 V vs Ag|AgCl, sat. KCl double junction reference electrode (Orion, Beverly, MA). Cyclic voltammetry (CV) was recorded in 30 μL supporting electrolyte (4 mM ammonium phosphate buffer, pH 7) dropped directly onto the surface of the clean WE; CE and MRE were immersed in the same droplet. CV was performed in the range from 0.050 to 0.500 V, typically at 10 mV s^{-1}. For electron-mediated studies, equimolar concentrations of benzoquinone and monensin (10−600 nM) were added externally to the vesicle system and new CVs were recorded. Concentrations were calculated based on sample reservoir volume. At the end of each experiment, the ferricyanide content of the vesicles was released by controlled potential electrolysis at −0.800 V for 10 s.

3. Results and Discussion

3.1. Vesicle Immobilization. Extruded vesicles encapsulating 1 mM $K_3Fe(CN)_6$ were prepared using the following lipid composition: 3 mol % PDP-$DC_{8,9}$PE as the minor lipid component and 97 mol % $DC_{8,9}$PC as the major lipid component. Stable vesicle dispersions were prepared by photopolymerization of the midchain diacetylenes. Structural characterization of the polymerized vesicle dispersion was assessed by transmission electron microscopy (Figure 2). TEM micrographs illustrate the structural stability of a typical polymerized vesicle sample (144 nm ± 55 nm, Figure 2), retaining its size, shape, and lamellarity upon exposure to a carbon copper grid as opposed to nonpolymerized samples (Supporting Information). Optimum conditions (i.e., sulfur content, polymerizing condition, and ferricyanide concentration) were established to avoid vesicle unraveling, agglomeration, or precipitation.

Polymerized vesicles containing disulfide functionalized PDP-$DC_{8,9}$PE that encapsulate 1 mM $K_3Fe(CN)_6$ were immobilized on gold surfaces. Using a quartz crystal microbalance (QCM), a frequency decrease was monitored over time (Figure 3A). Several QCM experiments were conducted which reproducibly revealed a frequency shift indicative of vesicle deposition. In Figure 3A, the frequency shift (Δf) of −72.3 Hz at 15 min is consistent with data published for intact vesicles immobilized on metallic surfaces such as Au,[18] Pt,[19] and TiO_2.[18] Figure 3A also demonstrates that the frequency shift is greatest for the initial deposition step, which is not surprising since maximum adsorption rates would occur for a completely bare, uncoated surface. From first principles, Dabros and van de Ven[20,21] derived a nonlinear phenomological expression for particle deposition (eq 1)

$$N_d = J_o\tau(1 - e^{-t/\tau}) \approx \Delta m_{tot}/A \quad (1)$$

where N_d, Δm, A, t, J_o, and τ represent surface coating density, total adsorbed mass to include vesicles, ferricyanide, and water, electrode area, time, initial particle flux, and a time constant that accounts for desorption and/or blocking effects, respectively. Using eq 1, a time constant of 7.46 min (correlation coefficient 0.9965) was computed by a nonlinear least-squares fit of the data in Figure 3A. For a fully coated vesicle surface, saturation is expected to occur within 5 time constants (37.3 min), which according to the random sequential adsorption theory[22] corresponds to a maximum fractional value of 0.547. Using the Sauerbrey equation,[23] a maximum total mass change of 37.44 ng is calculated for our system ($\Delta m = -C\Delta f$, where $C = 5.20 \times 10^{-13}$ kg/Hz).[24] Although the Sauerbrey equation correlates the amount of adsorbed mass to a frequency shift, it applies only to a system whereby the added mass is evenly distributed over the electrode and is much smaller than the weight of the quartz disk (i.e., $\Delta f/f \ll 1$).[25a] For vesicle-coated surfaces, deviations from the Sauerbrey model are known. Viscous losses derived from the immobilized vesicle layer (due to encapsulated ferricyanide and residual interstitial/intravesicular water) generate non-Sauerbrey behavior, which generally lead to lower measured frequency shifts. For more detailed discussions related to vesicle-induced viscous dissipation, the reader is referred to comprehensive work by Kasemo et al.[25]

Using atomic force microscopy (AFM), these vesicle-coated surfaces were inspected in air for their topography, structural integrity, dispersity, and surface density (Figure 3B). Figure 3B represents the final vesicle deposition step taken at 15 min in Figure 3A, whereby discrete spherical structures are observed. A measured coating density of 16.5 ± 1.5 vesicles/μm^2 corresponds to a calculated fractional surface coverage of 0.52, assuming a monodisperse population of 200 nm diameter vesicles.[26] In Figure 3B, structural compression and nonuniformity in vesicle size is visually apparent, having average longitudinal and latitudinal lengths of 365 ± 50 and 215 ± 35 nm, respectively. Due to surface attractive forces[27] and osmotic stress,[28] distortion of the vesicle structure is known to occur. Nonetheless, vesicle surface coverage is extensive over relatively large areas (>9 μm^2), but with no long-range, hexagonally close packed order. Also note that Figure 3B supports the assertion of vesicle stability on gold surfaces, since this image was taken 1 week after immobilization.

Using environmental scanning electron microscopy (ESEM), morphological information of these vesicle-coated surfaces was obtained in a hydrated environment (Supporting Information). ESEM provides additional evidence that these immobilized electroactive vesicles retain their size, structure, and shape on gold surfaces. Conducted within the ESEM chamber, energy dispersive spectroscopy (EDS) allows for chemical composition

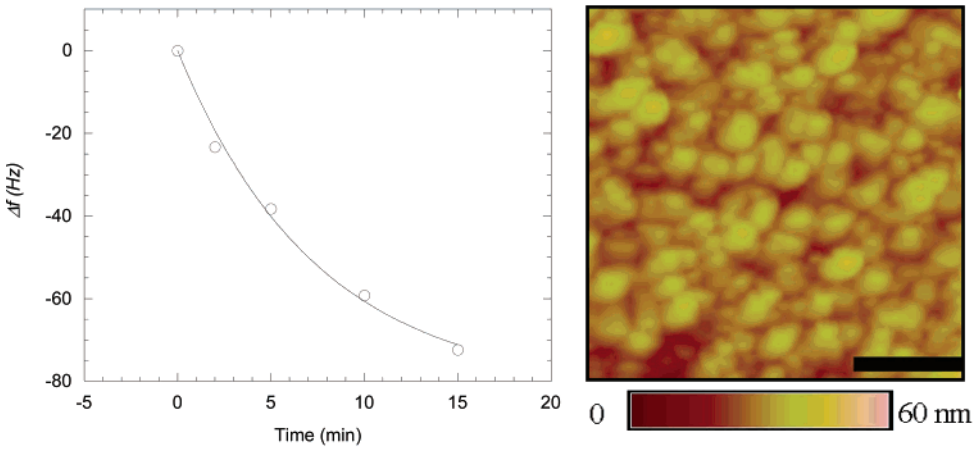

Figure 3. (A) QCM frequency shifts measured as a function of time for polymerized vesicles that encapsulate 1 mM $K_3Fe(CN)_6$ immobilized on a gold-coated quartz crystal resonator. (B) AFM image of polymerized vesicles that encapsulate 1 mM $K_3Fe(CN)_6$ immobilized on a gold-coated quartz crystal resonator. Bar represents 1 μm.

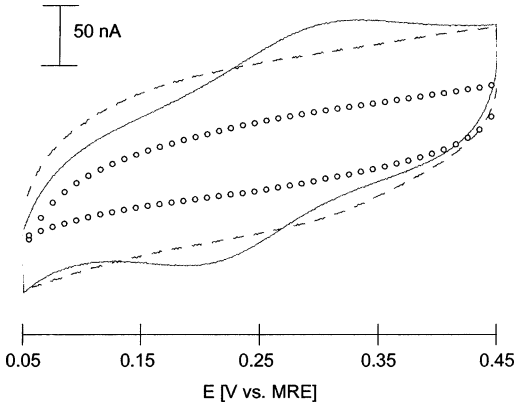

Figure 4. CV of buffer solution (dashed line) on bare gold disk electrode, illustrating a relatively large charging current. CV of polymerized vesicles encapsulating 1 mM $K_3Fe(CN)_6$ (circles) immobilized on the gold disk electrode, illustrating lack of faradaic activity and charging current suppression. CV of polymerized vesicles that encapsulate 1 mM $K_3Fe(CN)_6$ immobilized on gold disk electrode after electrolysis at -0.800 V for 10 s, illustrating release of entrapped ferricyanide (solid line). All scans were recorded at 10 mV s^{-1}.

analysis of these films (Supporting Information). The EDS spectrum displays the expected surface elements of gold ($M\alpha_1$ 2.123 keV and $M\beta_2$ 2.205 keV), silica ($K\alpha_1$ 1.7 keV), potassium ($K\alpha_1$ 3.3 keV) from desalting solutions, and phosphorus ($K\alpha_1$ 2.015 keV) from the phospholipid components of the vesicle bilayer. Sulfur ($K\alpha_1$ 2.31 keV) was not apparent in this spectrum due to such small quantities and signal overlap of the gold and phosphorus peaks. An iron peak was also not observed here. However, under similar processing conditions, a weak iron signal ($K\alpha_1$ 6.4 keV) was detected by X-ray fluorescence spectroscopy (Supporting Information).

3.2. Charge Capacity. The charge capacity of immobilized vesicles encapsulating 1 mM $Fe(CN)_6^{3-}$ (Figure 4, circles) was evaluated by cyclic voltammetry. Relative to the bare gold electrode in the same aqueous supporting electrolyte ($C_D \sim 5.7$ μF, Figure 4, dashed line), the double layer capacitance (C_D) for immobilized vesicles expectedly decreases ($C_D \sim 1.4$ μF). In Figure 4 (circles), ferricyanide external to the vesicles is not detected electrochemically (no faradaic signal present) and thus demonstrates that the vesicle bilayer functions as an insulating shell within this operating potential window. Note that this vesicle system is not impervious to $Fe(CN)_6^{3-}$ permeation. In the absence of an applied potential, a gradual increase in charging current was observed over several days (0.03 μF/h), which we attribute to passive permeation of entrapped $Fe(CN)_6^{3-}$.[29] Nonetheless, for relatively short times (i.e., within a day), immobilized electroactive vesicles withstood repetitive CV scans at 10 mV/s and remained stable up to an applied potential of -0.200 V; at more cathodic potentials, deterioration of the vesicle structure resulted in a measurable $Fe(CN)_6^{3-/4-}$ signal. Vesicle rupture and release of encapsulated ferricyanide was typically conducted at an applied potential of -0.800 V (Figure 4, solid line). (At this highly reductive potential, sulfhydryl/disulfide desorption from gold surfaces and deterioration of self-assembled monolayers are well documented.)[30] After this electrolytic step, CV reveals a faradaic signal with a midpoint potential ($E_{1/2}$) of 0.245 V coinciding with the midpoint potential of free $Fe(CN)_6^{3-/4-}$ ($E_{1/2} = 0.248$ V).[31] The interfacial structure at the electrode surface after electrolysis may be loosely interpreted from the separation of the anodic (oxidation) and cathodic (reduction) peak potentials. Theoretical predictions and empirical data encompass three common electrochemical scenarios:[32] (i) near 0 mV, (ii) near 60 mV per electron equivalent, and (iii) greater than 60 mV per electron equivalent peak separation corresponding to an immobilized redox species, to Nernstian electron transfer under diffusion control, and to sluggish kinetics imposed by a blocked or partially blocked surface, respectively.

In Figure 4 (solid line), the peak potential separation is 0.102 V, which suggests surface blocking derived from the vesicle bilayer membrane. On five separate electrodes, immobilized polymerized vesicles isolated entrapped $Fe(CN)_6^{3-}$ from the working electrode. Upon vesicle rupture at highly reductive potentials, free $Fe(CN)_6^{3-/4-}$ was detected having an average measured charge capacity of 58.2 ± 8 nC calculated from the integrated area under the anodic wave. Using Faraday's constant (96,486 C/mol), this corresponds to 6.03×10^{-13} mol, in reasonable agreement with calculations based upon AFM density measurements (2.23×10^{-13} mol)[33] and mass balances for complete surface coverage (2.36×10^{-13} mol).[34] These differences may be attributed to discrepancies in total inner vesicle volume calculated by assuming a single average vesicle diameter. Using a baseline-corrected peak anodic current of 14.35 nA, estimates based on the Randles−Sevcik equation for total electrolyzed ferricyanide (1.28×10^{-10} mol)[35] were deemed unrealistic. However, reasonable molar values could

be calculated by applying thin-layer electrochemical models for reversible (1.53×10^{-12} mol)[36] and totally irreversible (2.08×10^{-12} mol)[36] systems. Supported by these calculations, released $Fe(CN)_6^{3-/4-}$ appears to be partially confined near the electrode interface and overestimates may result from not satisfying the thin-layer criteria[37] in addition to numerical deviations accrued from a presumed nonuniform concentration profile, quasi-reversibility, and hemispherical system geometry. In our system, $Fe(CN)_6^{3-/4-}$ accessibility to the electrode and the complex structural nature at the electrode after vesicle rupture and electrolysis is still unknown. More experiments will be conducted for a later paper to elucidate a more accurate mechanism of the $Fe(CN)_6^{3-}$ release profiles and structural transformations occurring at the vesicle−electrode interface.

3.3. Mediated Charge Transport. Mediated charge transport, a phenomenon directly tied to the transduction of electrical energy, is widely found in biological systems.[38] For electron-mediated transport across vesicle membranes in the bulk phase, a tremendous amount of work exists in the literature.[1,2,39,40] Most closely related to our system is work conducted by Hinkle.[41] He demonstrated that benzoquinone (BQ) can effectively mediate electrons across the vesicle wall and that incorporation of cation mediators (ionophores) serves to enhance transport rates by attenuating opposing membrane potentials. Similar to Hinkle's work, we have also observed BQ-mediated electron transport across polymerized diacetylenic vesicle membranes in bulk phase with the incorporation of monensin[42] (a membrane-soluble cation carrier). External addition of lipophilic mediators does not appear to disrupt vesicle membranes: electron mediators such as BQ[41,43] and ferrocene,[41] metal ion carriers such as monensin, lasalocid, and calcimycin,[44] and sacrificial electron donors such as benzyl alcohol[45] have been reported to cross the vesicle wall without structural deterioration of the bilayer membrane. For electrons to cross vesicle membranes, three mechanisms[2a,40] have been proposed: (1) electron hopping, (2) electron tunneling, and (3) electron transport. Electron hopping does not seem likely in our system, since this would require a highly organized assembly of BQ mediators spanning the length of a polymerized vesicle bilayer membrane. With regard to electron tunneling, Hammarstrom[46] and Hurst[47] have resolved a detailed reaction mechanism for viologen redox chemistry and transport, eliminating the possibility of electron tunneling across a 3 nm thick phospholipid vesicle membrane. Using X-ray analysis, the vesicle wall thickness in our system measures 6.9 nm.[48] Our previous kinetic results agree with Hinkle's data and tend to support a diffusion-limited transport process.[43] Several examples exist in the literature whereby mediated transport of ions (electrons, cations, and anions) across the vesicle wall can be limited by transmembrane diffusion or, more accurately, membrane translocation rates.[4,49] For bulk phase systems,[2a,40] electron transport models have been reported that account for the cyclic turnover of BQ consisting of (1) electrochemical reactions occurring at the inner and outer aqueous/membrane interface and (2) translocation step(s) occurring within the vesicle bilayer membrane. In this report, we exploit what is known about bulk phase vesicle electrochemistry and transition these principles to a surface-immobilized vesicle system.

For vesicle membranes attached to metal surfaces, a simplified electron transport model is presented in Figure 5, schematically depicting the minimum steps required to achieve cyclic turnover of the membrane-bound mediator, BQ. Figure 5 illustrates an electrochemical two-electron/two-proton reaction at the electrode/vesicle membrane interface (step i) and at the inner vesicle membrane/solution interface (step iii). Translocation of the

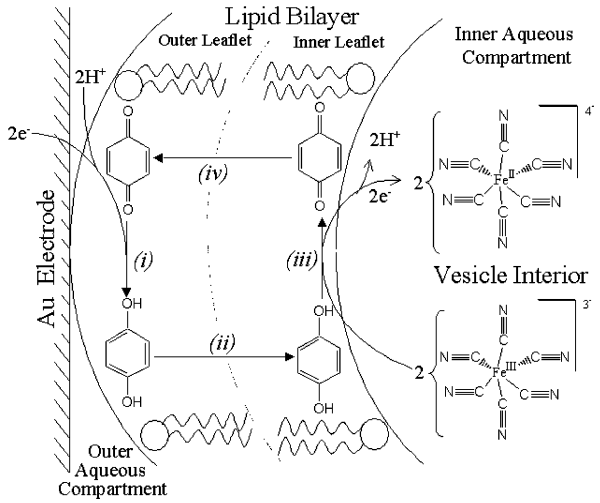

Figure 5. Electron transport model schematically depicting the minimum steps required to achieve cyclic turnover of the membrane-bound mediator. BQ is reduced at the electrode/vesicle membrane interface via a two-electron/two-proton electrochemical reaction (step i); H_2BQ, the reduced form of BQ, traverses the vesicle membrane (step ii); H_2BQ is oxidized (to regenerate BQ) at the inner vesicle membrane/solution interface via electrochemical reaction with vesicle-entrapped $Fe(CN)_6^{3-}$ and subsequent release of protons (step iii); finally, BQ traverses across the membrane to the electrode surface (step iv), completing one cycle of electron-mediated transport.

reduced (H_2BQ) and oxidized form of BQ is represented in steps ii and iv, respectively. Detailed heterogeneous electrochemistry of BQ (in the absence of vesicles) has been elegantly described by Laviron,[50] and at intermediate pH, elementary BQ reaction steps are known to follow the ECCE reaction sequence described in eq 2:[51]

$$BQ \xrightarrow{1} BQ^{\bullet -} \xrightarrow{2} HBQ^{\bullet} \xrightarrow{3} H_2BQ^{\bullet +} \xrightarrow{4} H_2BQ \qquad (2)$$

where steps 1, 2, 3, and 4 represent reduction, protonation, protonation, and reduction, successively. In our model (see Figure 5), interfacial elementary steps 1−4 in eq 2 are lumped as one effective reaction step. The redox reaction pathway depicted in Figure 5 is represented in eqs 3−6 as

$$BQ^{I} + 2H_I^{+} + 2e^{-} \rightarrow H_2BQ^{I} \qquad (3)$$

$$H_2BQ^{I} \rightarrow H_2BQ^{II} \qquad (4)$$

$$H_2BQ^{II} + 2Fe(CN)_6^{3-} \rightarrow BQ^{II} + 2Fe(CN)_6^{4-} + 2H_{II}^{+} \qquad (5)$$

$$BQ^{II} \rightarrow BQ^{I} \qquad (6)$$

where superscripts or subscripts I and II signify the outer membrane/electrode and inner membrane/solution interfaces, respectively. In this reaction scheme, H_2BQ mediates the transfer of both electrons and protons. In eq 3, electrons and protons are supplied from the working electrode and buffer solution, respectively. The overall reaction given in eq 7 (summing eqs 3−6)

$$Fe(CN)_6^{3-} + H_I^{+} + e^{-} \rightarrow Fe(CN)_6^{4-} + H_{II}^{+} \qquad (7)$$

accounts for ferricyanide reduction, proton pumping (into the vesicle interior), and electrical neutrality maintained by the working and counter electrodes.

Thermodynamic calculations predict and experiments verify that H_2BQ can reduce $Fe(CN)_6^{3-}$ (eq 5), since the formal

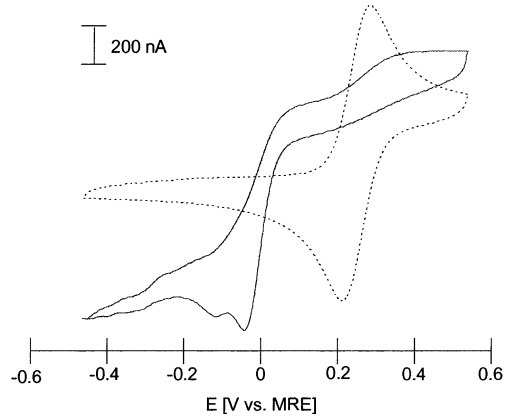

Figure 6. (A) BQ/H_2BQ (solid line) and $Fe(CN)_6^{3-/4-}$ (dotted line) electrochemistry at bare gold electrodes under ambient conditions buffered with sodium/hydrogen phosphate to pH 7. BQ and $Fe(CN)_6^{3-}$ initially at 94.4 μM and 77 μM, respectively. All scans were recorded at 50 mV s^{-1}.

potential of BQ/H_2BQ is more negative than $Fe(CN)_6^{3-/4-}$.[52] In Figure 6, BQ/H_2BQ (solid line) and $Fe(CN)_6^{3-/4-}$ (dotted line) voltammetry is shown under ambient conditions. Although in air the electrochemical behavior of BQ/H_2BQ is nonideal, an identifiable electrochemical signal is detected which can be used to monitor the anodic activity of the BQ/H_2BQ couple. As illustrated in Figure 6 (solid line), the anodic wave exhibits a broad and a substantially skewed electrochemical signal, whereas the cathodic wave displays a relatively sharper peak. In our system, H_2BQ oxidation and BQ reduction can be driven with an applied electrical potential of $E_{applied} \geq 0.380$ V and $E_{applied} \leq -0.100$ V, respectively. For eq 5 to proceed in reverse, significant electronic coupling between BQ and $Fe(CN)_6^{4-}$ is required.[53] From the electrochemical data provided in Figure 6, signal overlap between BQ/H_2BQ (solid line) and $Fe(CN)_6^{3-/4-}$ (dotted line) is evident. Due to the relative positions of the BQ/H_2BQ and $Fe(CN)_6^{3-/4-}$ redox couples, quasi-revesible charge transfer can be exploited in this system. To reiterate, BQ/H_2BQ and $Fe(CN)_6^{3-/4-}$ are both chemically reversible as individual redox couples; the reaction direction of eq 3 can be controlled by the potential applied to the working electrode (i.e., adjusting the Fermi level); eq 5 is thermodynamically favorable at pH 7 and its reversibility depends on the degree of electronic coupling between BQ and $Fe(CN)_6^{4-}$.

The quasi-reversible nature of BQ/H_2BQ and the expected position of the formal potential reported here (Figure 6) agree with published voltammetry. For comparison, several investigators have reported quasi-reversible charge transfer of BQ/H_2BQ on bare and SAM coated surfaces,[54] except for Shim's work[55] demonstrating a reversible 30 mV peak potential separation on bare Au. Extensive work conducted by Hubbard and Soriaga[56] detail geometrical interactions with gold surfaces, affecting BQ formal potential.[57] Surface immobilized BQ having sulfhydryl functionality (an electron-withdrawing group) has been reported to significantly affect BQ formal potential due to resonance stabilization.[58] Most closely related to our work are phospholipid cast-layer electrodes studied by Park,[59] which provides insight into the influence of the lipid environment on BQ/H_2BQ electrochemistry. On glassy carbon electrodes, they report a clear H_2BQ oxidation signal at 0.360 V and 0.230 V vs Ag|AgCl when in the presence of moderate length dilauroyl phospholipids with and without a benzonitrile precursor layer, respectively. They conclude that BQ interacts significantly via "hydration" of the lipid phosphate group (i.e., $-$P(O)OH), producing the HBQ• radical. With freely available H^+ from solution or neighboring phosphate-bearing lipids, H_2BQ was determined to readily form. For dilauroyl phospholipid coated electrodes, they[59] report BQ reduction at -0.042 V vs Ag|AgCl.

Holding the electrode potential at relatively large (cathodic) overpotentials is not an uncommon technique for evaluating BQ redox electrochemistry.[58,59] In our system (Figure 7A), we precondition the immobilized vesicle assembly at -0.200 V for 10 s and then scan in a potential window ($0.100-0.500$ V), where quinone oxidation was previously observed (Figure 6). As shown in Figure 7A (solid line, □), charge transfer is observed when immobilized polymerized vesicles that encapsulate 1 mM $Fe(CN)_6^{3-}$ are doped at equimolar levels with 250 nM BQ and monensin. The peak potential of the anodic wave (0.318 V)[60] coincides with the reported and observed formal potential of free BQ (Figure 6). Subtraction of the background scan (Figure 7A, solid line) from the BQ-mediated system (Figure 7A, solid line, □) leads to well-defined anodic voltammetry (Figure 7B, dashed line). We assign the observed electrochemical signal to the oxidation of H_2BQ or of a reduced intermediate (refer to eq 2).

From Figure 7A (solid line, □) and Figure 7B (dashed line), the overall measured current is derived from direct oxidation of the reduced quinone in addition to the oxidation of encapsulated ferrocyanide as mediated by the BQ/H_2BQ transport process. Note that the cathodic wave in Figure 7A (solid line, □) does not display a recognizable BQ reduction wave, since this electrochemical reaction is outside the recorded voltammogram. To verify that $Fe(CN)_6^{3-/4-}$ is indeed present, the vesicle-immobilized system was poised at -0.800 V, a potential that can rupture the vesicle membrane and trigger the release of internal $Fe(CN)_6^{3-/4-}$. Under this electrochemically aggressive condition, the inner voltammogram (Figure 7A, solid line, □) widens with concomitant peak broadening (Figure 7A, dashed line, △). Anodic current begins to flow at 0.16 V and depletes slightly at 0.45 V. Figure 7A (dashed line, △) reveals complex voltammetry for the multicomponent BQ/H_2BQ and $Fe(CN)_6^{3-/4-}$ system. However, scan deconvolution via background subtraction (Figure 7B, solid line) demonstrates the presence of a redox couple corresponding to the formal potential of $Fe(CN)_6^{3-/4-}$. In Figure 7B (solid line), a peak potential more negative than the observed anodic wave recorded prior to electrolysis (Figure 7A, solid line, □) advocates for mediated charge transport across the vesicle membrane occurring at BQ/H_2BQ formal potential. The amount of charge transferred (i.e., the faradaic signal) after preconditioning is calculated from the area under the anodic H_2BQ wave, which for Figure 7A (solid line, □) corresponds to 53.6 nC.

Control experiments were conducted to address the electrochemical activity of BQ/monensin in the absence of $Fe(CN)_6^{3-}$ and of BQ only in the presence of vesicle-entrapped $Fe(CN)_6^{3-}$.[61] A plot of anodic faradaic charge as a function of BQ/monensin concentration in the presence of immobilized polymerized vesicles containing water only (no ferricyanide) yields a slope of 0.005 nC/nM (Figure 8, solid line, circles). From Figure 7A (solid line, □), the measured faradaic signal is 53.6 nC, which is greater than the electroactivity expected for 250 nM BQ (0.005 nC/nM $\times$ 250 nM $=$ 1.25 nC). The remaining charge (52.4 nC) is accounted for by electrons supplied from previously reduced ferricyanide produced during a 10 s preconditioning interval at -0.200 V (a potential which does not affect the structural integrity of IPEVs). CVs were recorded for IPEVs at varying BQ concentrations (as in Figure 7). A nonlinear relationship was observed for mediated electron transport of IPEVs as a function of BQ/monensin concentration (Figure 8,

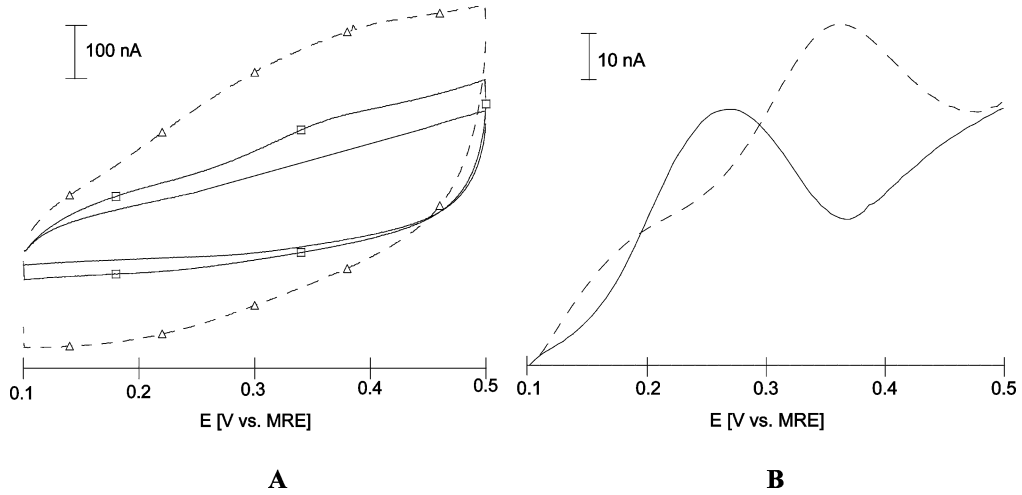

Figure 7. (A) CV (solid line) of polymerized vesicles that that encapsulate 1 mM $K_3Fe(CN)_6$ immobilized on gold disk electrode. CV (solid line, □) of the same polymerized vesicles that encapsulate 1 mM $K_3Fe(CN)_6$ immobilized on gold disk electrode after doping with 250 nM benzoquinone and monensin (equimolar concentrations based on reservoir volume), illustrating electron-mediated transport at the formal potential of benzoquinone. CV (dashed line, △) of the same immobilized polymerized vesicle sample after electrolysis at −0.800 V for 10 s. (B) Scan deconvolution of CV in (A) demonstrates the presence of benzoquinone (dashed line) and ferricyanide (solid line) after vesicle rupture. All scans were recorded at 10 mV s^{-1}.

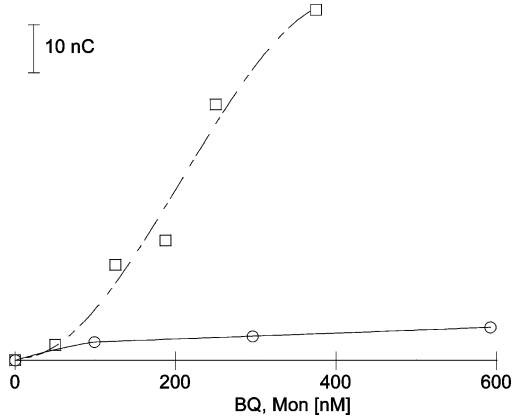

Figure 8. Anodic charge transfer (dashed line, □) measured from CV of electron-mediated IPEVs as a function of equimolar concentrations of benzoquinone and monensin (concentrations based on reservoir volume). Anodic charge transfer (solid line, ○) is plotted as a function of equimolar concentrations of benzoquinone and monensin (based on reservoir volume) in the presence of immobilized polymerized vesicles that contain only water.

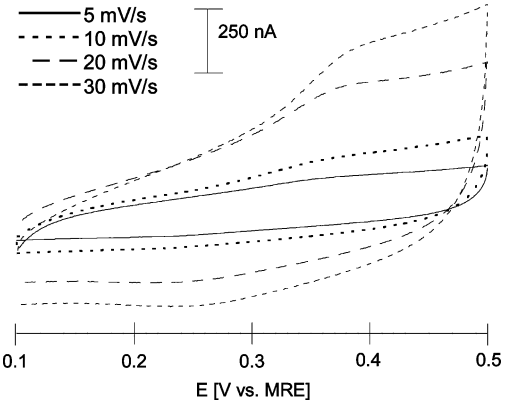

Figure 9. CV (refer to Figure 7A, solid line, □) of polymerized vesicles immobilized on gold disk electrode that encapsulate 1 mM $K_3Fe(CN)_6$ doped with 250 nM benzoquinone and monensin (based on reservoir volume) as a function of increasing scan rate. Least-squares fit of the anodic peak currents versus scan rate gives an exponent dependence on scan rate of 0.85, supporting a nonmobile (rather than a freely diffusing) electron mediator.

dashed line, □). At relatively low BQ/monensin concentrations (<50 nM), charge transport is ineffective whereas electron exchange between vesicle-entrapped $Fe(CN)_6^{3-/4-}$ and the electrode is enhanced at higher BQ/monensin concentrations (>50 nM).[62] For moderate BQ/monensin concentrations (50−400 nM), IPEV oxidation increases linearly with mediator concentration. Figure 8 displays the amount of charge that can be transferred (oxidized) from IPEVs as a function of BQ/monensin concentration. However, for a specified BQ concentration, charge transport (i.e., current flow) is directly related to the mediator turnover rate, which depends kinetically on reaction and mass transfer rates (i.e., the Damkholer number).[63] Previously evaluated in the bulk phase, BQ-mediated electron transport across polymerized diacetylenic vesicle membranes was found to be transport limited (average translocation rate 0.06 s^{-1}).[43] With reference to Figure 7A (solid line, □), the baseline-corrected anodic peak current of 17 nA corresponds to only 40% of the maximum current achievable when operating at maximum velocity.[64] From Figures 7 and 8, one can conclude that BQ accessibility to the electrode and its translocation rate across the vesicle membrane significantly affect electron transport to and from IPEVs.

To further evaluate electron transport mediated by BQ for IPEVs, a voltammetric scan rate study was performed (Figure 9). Anodic peak currents plotted as a function of scan rate showed an exponent dependence to the power of 0.85. Since theory[32] predicts a square-root dependence for diffusive redox species (i.e., Randles−Sevcik equation) and a linear dependence for immobilized redox species, a scan rate exponent between 0.5 and 1.0 is expected. A scan rate exponent of 0.85 indicates that BQ displays immobile (membrane-confined) rather than diffusive properties. Due to the hydrophobic nature of the mediator,[65] BQ partitions more readily in the vesicle membrane than in the aqueous phases, which is consistent with the observed scan rate dependence. In Figure 9, a broad anodic signal was observed at relatively slower scan rates (5−10 mV s^{-1}) having a peak potential near 0.318 V.[60] At higher scan rates (20−30 mV s^{-1}), sharper peak resolution and peak shifting was observed. This would indicate that a relatively larger number of chemical states and/or pathways may exist at slower scan rates for electron-mediated transport via BQ.[40,66] From the results

in Figure 9, IPEVs demonstrate that electron exchange can be localized at a vesicle membrane/electrode interface.

4. Conclusion

Immobilized vesicles composed of diacetylenic phospholipids were shown to be stable on gold surfaces. The amount of electroactive material (e.g., ferricyanide) encapsulated within the vesicle core establishes the system's charge capacity. In the presence of 1,4-benzoquinone (a lipophilic electron mediator), electron exchange across the vesicle bilayer membrane was observed. The extent of charge transfer is governed by the electron mediator 1,4-benzoquinone, increasing nonlinearly with concentration. These findings demonstrate a method for potentially developing electrodes at the submicron scale using bioderived components and principles.

Acknowledgment. This work is supported by ONR and DARPA. We thank Dr. L. M. Tender, Dr. S. Jhaveri, and Dr. S. A. Trammell at NRL for insightful electrochemical discussions.

Supporting Information Available: TEM and ESEM micrographs with spectroscopic data of elemental composition provide additional characterization of IPEVs. This material is available free of charge via the Internet at http://pubs.acs.org.

References and Notes

(1) (a) Mueller, A.; O'Brien, D. F. *Chem. Rev.* **2002**, *102*, 727. (b) Ringsdorf, H.; Schlarb, B.; Venzmer, J. *Angew. Chem., Int. Ed. Engl.* **1988**, *27*, 113.

(2) (a) Fendler, J. H. *Membrane mimetic chemistry* Wiley-Interscience: New York, 1982. (b) Lasic, D. D. *Liposomes: From physics to applications* Elsevier: New York, 1993.

(3) Stanish, I.; Lowy, D. A.; Tender, L. M.; Singh, A. *J. Phys. Chem. B* **2002**, *106*, 3503.

(4) (a) Khairutdinov, R. F.; Hurst, J. K. *Nature* **1999**, *402*, 509. (b) Kurihara, K.; Fendler, J. H. *J. Am. Chem. Soc.* **1983**, *105*, 6152.

(5) Tundo, P.; Kurihara, K.; Kippenberger, D. J.; Politi, M.; Fendler, J. H. *Angew. Chem., Int. Ed. Engl.* **1982**, *21*, 81.

(6) (a) Kugimiya, S.; Lazrak, T.; Blanchard-Desce, M.; Lehn, J.-M. *J. Chem. Soc., Chem. Commun.* **1991**, *17*, 1179. (b) Kobuke, Y.; Yamanishi, M.; Hamachi, I.; Kagawa, H.; Ogoshi, H. *J. Chem. Soc., Chem. Commun.* **1991**, *13*, 895.

(7) Tien, H. T.; Salamon, Z.; Ottova, A. *Biomed. Eng.* **1991**, *18*, 323.

(8) Yoshina-Isihi, C.; Boxer, S. G. *J. Am. Chem. Soc.* **2003**, *125*, 3696.

(9) Katagiri, K.; Hamasaki, R.; Ariga, K.; Kikuchi, J.-I. *J. Am. Chem. Soc.* **2002**, *124*, 7892.

(10) Jung, L. S.; Schumaker-Perry, J. S.; Campbell, C. T.; Yee, S. S.; Gelb, M. H. *J. Am. Chem. Soc.* **2000**, *122*, 4177.

(11) Yang, Q.; Wallstne, M.; Ludahl, P. *Biochim. Biophys. Acta* **1988**, *938*, 243.

(12) Keller, C. A.; Kasemo, B. *Biophys. J.* **1998**, *75*, 1397.

(13) (a) Stanish, I.; Santos, J. P.; Singh, A. *J. Am. Chem. Soc.* **2001**, *123*, 1008. (b) Stanish, I.; Ray, R. I.; Singh, A. *Mater. Res. Soc. Symp. Proc.* **2002**, *711*, 101.

(14) Johnston, D. S.; Sanghera, S.; Pons, M.; Chapman, D. *Biochim. Biophys. Acta* **1980**, *602*, 57.

(15) Martin, F. J.; Papahadjopoulos, D. P.; Hubbell, W. L. Thiol Reactive Liposomes. U.S. Patent 4,429,008, 1984.

(16) Singh, A.; Schnur, J. M. In *Phospholipids Handbook* Cevc, G., Ed.; Marcel Dekker: New York, 1993; pp 233−291.

(17) (a) Ciobanu, M.; Wilburn, J. B.; Buss, N. I.; Ditavong, P.; Lowy, D. A. *Electroanalysis* **2002**, *14*, 989. (b) Ciobanu, M.; Wilburn, J. B.; Lowy, D. A. *Electroanalysis*, in press.

(18) (a) Reimhult, E.; Hook, F.; Kasemo, B. *Langmuir* **2003**, *19*, 1681. (b) Keller, C. A.; Kasemo, B. *Biophys. J.* **1998**, *75*, 1397. (c) Rodahl, M.; Hook, F.; Fredrikson, C.; Keller, C. A.; Krozer, A.; Brzezinski, P.; Voinova, M.; Kasemo, B. *Faraday Discuss.* **1997**, *107*, 229.

(19) Tjarnhage, T.; Puu, G. *Colloids Surf. B* **1996**, *8*, 39.

(20) (a) Dabros, T.; van de Ven, T. G. M. *J. Colloid Interface Sci* **1982**, *89*, 232. (b) van de Ven, T. G. M. *Colloid Surf. A* **1998**, *13*, 207.

(21) Tragardh, C.; Joscelyne, S. *J. Colloid Interface Sci.* **1997**, *192*, 294.

(22) (a) Viot, P.; Tarjus, G.; Ricci, S. M.; Talbot, J. *J. Chem. Phys.* **1992**, *97*, 5212. (b) Semmler, M.; Mann, E. K.; Ricka, J.; Borkovec, M. *Langmuir* **1998**, *14*, 5127.

(23) Sauerbrey, G. *Z. Phys.* **1959**, *155*, 206.

(24) $\Delta f = (-2/\sqrt{\mu_q \rho_q})(f_o^2/A)\Delta m$, where f_o, A, ρ_q, and μ_q represent the fundamental resonant frequency (9×10^6 Hz), surface area (9.51×10^{-6} m^2), quartz density (2.65×10^3 kg/m^3), and quartz shear modulus (2.957×10^{10} N/m^2), respectively.

(25) (a) Rodahl, M.; Hook, F.; Krozer, A.; Brzezinski, P.; Kasemo, B. *Rev. Sci. Instrum.* **1995**, *66*, 3924. (b) Rodahl, M.; Kasemo, B. *Sens. Actuators, A—Phys.* **1996**, *54*, 448. (c) Voinova, M. V.; Rodhal, M.; Jonson, M.; Kasemo, B. *Phys. Scr.* **1999**, *59*, 391. (d) Rodahl, M.; Hook, F.; Kasemo, B. *Anal. Chem.* **1996**, *68*, 2219. (e) Rodhal, M., Kasemo, B. *Rev. Sci. Instrum.* **1996**, *67*, 3238.

(26) $N_{ves} \times$ vesicle cross-sectional area/substrate area = 16.5 vesicles/μm$^2 \times 10^8$ μm^2/cm$^2 \times \pi R^2 = 1.65 \times 10^9$ vesicles/cm$^2 \times \pi(200/2 \times 10^{-7}$ cm$)^2 = 0.52$.

(27) Reimhult, E.; Hook, F.; Kasemo, B. *J. Chem. Phys.* **2002**, *117*, 7401.

(28) (a) Parsegian, V. A.; Fuller, N.; Rand, R. P. *Proc. Natl. Acad. Sci. U.S.A.* **1979**, *76*, 2750 (b) Ito, T.; Yamazaki, M.; Ohnihi, S.-I. *Biochemistry* **1989**, *28*, 5626.

(29) Bulk phase studies at pH 7 revealed a half-life of 2.4 weeks for $Fe(CN)_6^{3-}$ permeation across diacetylenic vesicles (refer to ref 3).

(30) (a) Finklea, H. O.; Avery, S., Lynch, M. *Langmuir* **1987**, *3*, 409. (b) Porter, M. D.; Bright, T. B.; Allara, D. L.; Chidsey, C. E. D. *J. Am. Chem. Soc.* **1987**, *109*, 3559. (c) Madueno, R.; Sevilla, J. M.; Pineda, T.; Roman, A. J.; Blazques, M. *J. Electroanal. Chem.* **2001**, *506*, 92.

(31) Determined experimentally in bulk phase (refer to Figure 6).

(32) Bard, A. J.; Faulkner, L. R. *Electrochemical Methods*; John Wiley & Sons: New York, 2001.

(33) Refer to ref 26. N_{ves}/area $\times$ electrode area $\times$ vesicle inner volume (for $R_o = 100$ nm) $\times$ ferricyanide concentration $= 1.65 \times 10^9$ cm$^{-2} \times 0.04$ cm$^2 \times 3.38 \times 10^{-15}$ cm$^3 \times 10^{-6}$ mol/cm$^3 = 2.23 \times 10^{-13}$ mol.

(34) Refer to refs 3 and 22. N_{ves} ($0.547 \times$ electrode area/vesicle cross-sectional area for $R_o = 100$ nm) $\times$ vesicle inner volume (for $R_o = 100$ nm) $\times$ ferricyanide concentration $= 0.547 \times 0.04$ cm$^2/\pi(200/2 \times 10^{-7}$ cm$)^2 \times 3.38 \times 10^{-15}$ cm$^3 \times 10^{-6}$ mol/cm$^3 = 2.36 \times 10^{-13}$ mol.

(35) Refer to ref 32. $i_p = 2.69 \times 10^5 n^{3/2} A D_o^{1/2} \upsilon^{1/2} C_o^*$. $A = 0.04$ cm^2, $n = 1$, $D_o = 0.98 \times 10^{-5}$cm^2/s, $\upsilon = 0.01$ V/s, and system volume $= 30 \times 10^{-6}$ L. C_o^* is in units of mol/cm^3.

(36) Refer to ref 32. $i_p = 9.39 \times 10^5 n^2 \upsilon V C_o^*$ (reversible) and $i_{p,c} = n\alpha n_a F^2 \upsilon V C_o / 2.718RT$ (totally irreversible), where $V = 30 \times 10^{-3}$ cm^3, $F = 96{,}486$ C/mol, $n = 1$, $R = 8.314$ J/(mol·K), $T = 298$ K, and $\alpha = 0.5$.

(37) Thin layer condition $l \ll \sqrt{2Dt}$; l (electrode diameter) $= 0.226$ cm and $\sqrt{2Dt} = \sqrt{2 \times 0.98 \times 10^{-5}\text{cm}^2/\text{s} \times 100\text{s}} = 0.002$ cm.

(38) Voet, D. *Fundamentals of Biochemistry*; John Wiley & Sons: New York, 1999.

(39) Gregoriadis, G. *Liposome Technology*; CRC Press: Boca Raton, FL, 1993; Vol. 1-3.

(40) Robinson, J. N.; Cole-Hamilton, D. J. *Chem. Soc. Rev.* **1991**, *20*, 49.

(41) Hinkle, P. *Biochem. Biophys Res. Commun.* **1970**, *41*, 1375.

(42) Cox, B. G.; Schneider, H. *Coordination and Transport Properties of Macrocyclic Compounds in Solution*; Elsevier Science Publishing Co. Inc.: New York, 1992.

(43) Stanish, I.; Singh, A. *Mater. Res. Soc. Symp. Proc.* **2002**, *711*, 333.

(44) (a) Stanish, I.; Monbouquette, H. G. *J. Membr. Sci.* **2001**, *192*, 99. (b) Stanish, I. Thermodynamic and Kinetic Tuning of Metal-Sorbing Vesicle Selectivity for the Recovery of Toxic Metal Ions. Dissertation, UCLA, 1999.

(45) Horvath, O. *Langmuir* **1999**, *15*, 279.

(46) Hammarstrom, L.; Almgren, M.; Norrby *J. Phys. Chem.* **1992**, *96*, 5017.

(47) (a) Patterson, B. C.; Thompson, D. H.; Hurst, J. K. *J. Am. Chem. Soc.* **1988**, *110*, 3656. (b) Lymar, S. V.; Hurst, J. K. *J. Phys. Chem.* **1994**, *98*, 898.

(48) Rhodes, D. G.; Singh, A. *Chem. Phys. Lipids* **1991**, *59*, 215.

(49) (a) Lauger, P. *Nature* **1972**, *17*, 24. (b) O'Brien, D. F. *Photochem. Photobiol.* **1979**, *29*, 679.

(50) Laviron, I. *J. Electroanal. Chem.* **1983**, *146*, 15.

(51) (a) Evans, D. H. *Chem. Rev.* **1990**, *90*, 739. (b) Chambers, J. Q. In *The Chemistry of Quinoid Compouds*; Patai, S., Rappoport, Z., Eds.; Wiley: New York, 1988; p 719.

(52) Angell, D. H.; Dickinso, T. *J. Electroanal. Chem.* **1966**, *16*, 103.

(53) (a) Barbara, P. F.; Meyer, T. J.; Ratner, M. A. *J. Phys. Chem.* **1996**, *100*, 13148. (b) Moser, C. C.; Keske, J. M.; Warncke, K.; Farid, R. S.; Dutton, P. L. *Nature* **1992**, *355*, 796. (c) Marcus, R. A.; Sutin, N. *Biochim. Biophys. Acta.* **1985**, *811*, 265.

(54) (a) Shaidarova, L. G.; Geddimina, A. V.; Budnikov, G. K. *J. Anal. Chem.* **2003**, *58*, 193. (b) Kinnear, K. T.; Monbouquette, H. G. *Anal. Chem.* **1997**, *69*, 1771. (c) Gupta, N.; Linschitz, H. *J. Am. Chem. Soc.* **1997**, *119*, 6384. (d) Krysinski, P.; Brzostowska-Smolska, M. *J. Electroanal. Chem.* **1997**, *424*, 61. (e) Mandic, Z.; Duic, L. *J. Electroanal. Chem.* **1996**, *403*, 133. (f) Chailapakul, O.; Crooks, R. M. *Langmuir* **1993**, *9*, 884.

(55) Shim, Y.-B.; Park, S.-M. *J. Electroanal. Chem.* **1997**, *425*, 201.

(56) (a) Soriaga, M. P.; Hubbard, A. T. *J. Am. Chem. Soc.* **1982**, *104*, 3937. (b) Temesghen, W.; Jeng, J.-J., Carrasquillo, A.; Soriaga, M. P. *Langmuir* **1994**, *10*, 3929.

(57) BQ reversibly adsorbs/desorbs on bare Au as opposed to Pt surfaces. Bravo, B. G.; Mebrahtu, T.; Soriaga, M. P.; Zapien, D. C.; Hubbard, A. T.; Stickney, J. L. *Langmuir* **1987**, *3*, 595.

(58) Sato, Y.; Fujita, M.; Mizutani, F.; Uosaki, K. *J. Electroanal. Chem.* **1996**, *409*, 145.

(59) (a) Park, H.; Higuchi, T.; Okazaki, S.; Oyama, M. *J. Electroanal. Chem.* **2002**, *518*, 27. (b) Park, H.; Oyama, M.; Shim, Y.-B.; Okazaki, S. *J. Electroanal. Chem.* **2000**, *484*, 131. (c) Park, H.; Park, J.-S.; Shim, Y.-B. *J. Electroanal. Chem.* **1997**, *438*, 113.

(60) Calculated by taking the first derivative of the anodic wave.

(61) For control experiments performed in the absence of monensin, BQ mediated charge transport displayed approximately a 2-fold decrease in signal.

(62) Stanish, I.; Lowy, D. A.; Singh, A. *Mater. Res. Soc. Symp. Proc.* **2003**, *775*, 5.4.1.

(63) Bailey, J. E.; Ollis, D. F. *Biochemical Engineering Fundamentals*, 2nd ed.; McGraw-Hill: New York, 1986.

(64) $0.06\ s^{-1} \times 250\ nM \times 30 \times 10^{-6}\ L \times 96486\ C\ mol^{-1} = 43\ nA$.

(65) (a) Hennsen, B. L.; Achine, L.; Ruvalcaba, N. M.; Ortiz, A.; Hernandez, J.; Farfan, N.; Aguilar-Martinez, M. *J. Agric. Food Chem.* **1998**, *46*, 724. (b) Log(Kp) values for hydroquinone and benzoquinone in octanol/water (membrane mimicking conditions) are 0.59 and 0.2, respectively (http://toxnet.nlm.nih.gov).

(66) Stein, W. D. *Transport and Diffusion across Cell Membranes*; Academic Press: Orlando, FL, 1986.